Available online at www.eccomasproceedia.org
Eccomas Proceedia COMPDYN (2017) 802-814

ECCOMAS
Proceedia

COMPDYN 2017
6th ECCOMAS Thematic Conference on
Computational Methods in Structural Dynamics and Earthquake Engineering
M. Papadrakakis, M. Fragiadakis (eds.)
Rhodes Island, Greece, 15–17 June 2017

# FINITE ELEMENT ANALYSES ON FREE FROM DAMAGE SEISMIC RESISTING BEAM-TO-COLUMN JOINTS

**Mario D'Aniello[1], Mariana Zimbru[1], Raffaele Landolfo[1], Massimo Latour[2], Gianvittorio Rizzano[2] and Vincenzo Piluso[2]**

[1] University of Naples 'Federico II', Department of Structures for Engineering and Architecture
Via Forno Vecchio 36, Naples 80134, Italy
mdaniel@unina.it, mariana.zimbru@unina.it, landolfo@unina.it

[2] University of Salerno, Department of Civil Engineering
Via Giovanni Paolo II, 132, Fisciano, Italy
mlatour@unisa.it, g.rizzano@unisa.it, v.piluso@unisa.it

**Keywords:** Free from damage joints, Steel structures, Finite element analyses, Seismic design.

**Abstract.** *The seismic design strategy implemented in current codes is based on the capacity design principles that allow the formation of plastic hinges into predefined parts of the structure. Therefore, significant damage is expected at ultimate limit state, to which high repair costs are associated. Recently, new design strategies have been proposed in order to avoid the damage of the structure. The most of them are grouped into two categories, namely i) using special damping devices introduced in the structure as additional resisting element; ii) changing the dissipation mechanism of the structure by means of friction-based dissipative joints. The second possibility is promising and really effective because it guarantees no architectural interference if adopted for moment-resisting frames (MRFs), and low forces transferred to the foundations. The novelty of free from damage (FREEDAM) joints lays in the fact that the energy is dissipated by friction at the interface between plates in contact instead of the classical plastic deformation energy dissipation mechanism. In this paper, the seismic behaviour of FREEDAM joints is investigated by means of parametric finite element analyses carried out in order to examine the influence of geometric and mechanical feature of the friction device (e.g. position of friction plane, type of friction interface, bolt clamping, bolt strength). The accuracy of finite element models is also validated on the basis of some experimental tests.*


Peer-review under responsibility of the organizing committee of COMPDYN 2017.
doi: 10.7712/120117.5458.17524

# 1 INTRODUCTION

The current seismic design procedures are based on the philosophy of hierarchy of resistances that aims at achieving ductile and dissipative plastic mechanisms with relatively low constructional costs [1-8]. Although effective and economically advantageous at the construction stage, the capacity design philosophy applied to traditional structural systems requires structural damages after seismic events, thus leading to significant economic losses [9-13].

Therefore, worldwide research effort is currently devoted to improve the traditional structural systems as well as to develop cost effective alternatives to eliminate or limit and localize the damage, such as buckling restrained braces (BRBs) [14-17], shear metal panels [18, 19], viscous dampers [20-22], replaceable shear links in eccentrically braced frames (EBFs) [23,26] and dissipative joints [27-32].

The concept of free from damage structures using friction-based devices has become very appealing and promising in the last decades [33, 40].

In Europe, this concept is currently under investigation within the ongoing research project FREEDAM (FREE from DAMage steel connections) [41]. This project aims at developing and seismically prequalifies novel types of steel joints that dissipate the seismic energy by means of friction at the level of surfaces in contact clamped by preloaded bolts and specifically designed to undergo relative sliding at a given force level. The cyclic behaviour of these joints is stable with low degradation, even though it depends on the friction material used at the sliding interface [36-40].

Figure 1 depicts the two main typologies of the joints tested within [41]. As it can be noted, the main difference is the shape of the friction damper (horizontal and vertical, respectively). In particular, the sliding part of the friction damper is detailed with slotted holes that allow it the slippage with respect to the fixed parts (friction pads and L-stubs). Under bending actions, both joint configurations rotate around the centre of compression, which is located in the mid thickness of the Tee web under hogging and in the mid distance between the L-stubs/bolts of the damper under sagging. Therefore, in order to avoid the damage of steel components, those elements should be designed to resist the maximum forces transferred by the friction damper under both static and dynamic slippage.

The required design strength of FREEDAM joints can be easily obtained by calibrating the slippage force of the friction damper. The slippage force is computed as the product of the friction coefficient (which is a mechanical feature of the interface between the friction pads and the haunch), the number of friction interfaces (e.g. two in case of a symmetrical damper) and the sum of the pre-tightening forces applied by means of preloaded bolts. All these factors influence the bending capacity of the joints. Therefore, a parametric study based on finite element analyses are carried out and the results are presented and discussed in this paper.

# 2 FINITE ELEMENT MODEL

## 2.1 Modelling Assumptions

Abaqus v6.14 [42] is used to carry out the finite element simulations. The geometrical features of the examined joints are reported in Figure 1. Structured mesh technique is used and the finite element type C3D8R (an 8-node linear brick with reduced integration) is adopted for steel beams, columns and high strength bolts.

The average properties of S355 steel grade are assumed [6]. The yielding is modelled by means of the von Mises yield criteria. Plastic hardening is represented using a combined isotropic and kinematic hardening.

HV 10.9 grade pre-loadable bolts are considered and modelled as reported by [6, 43].

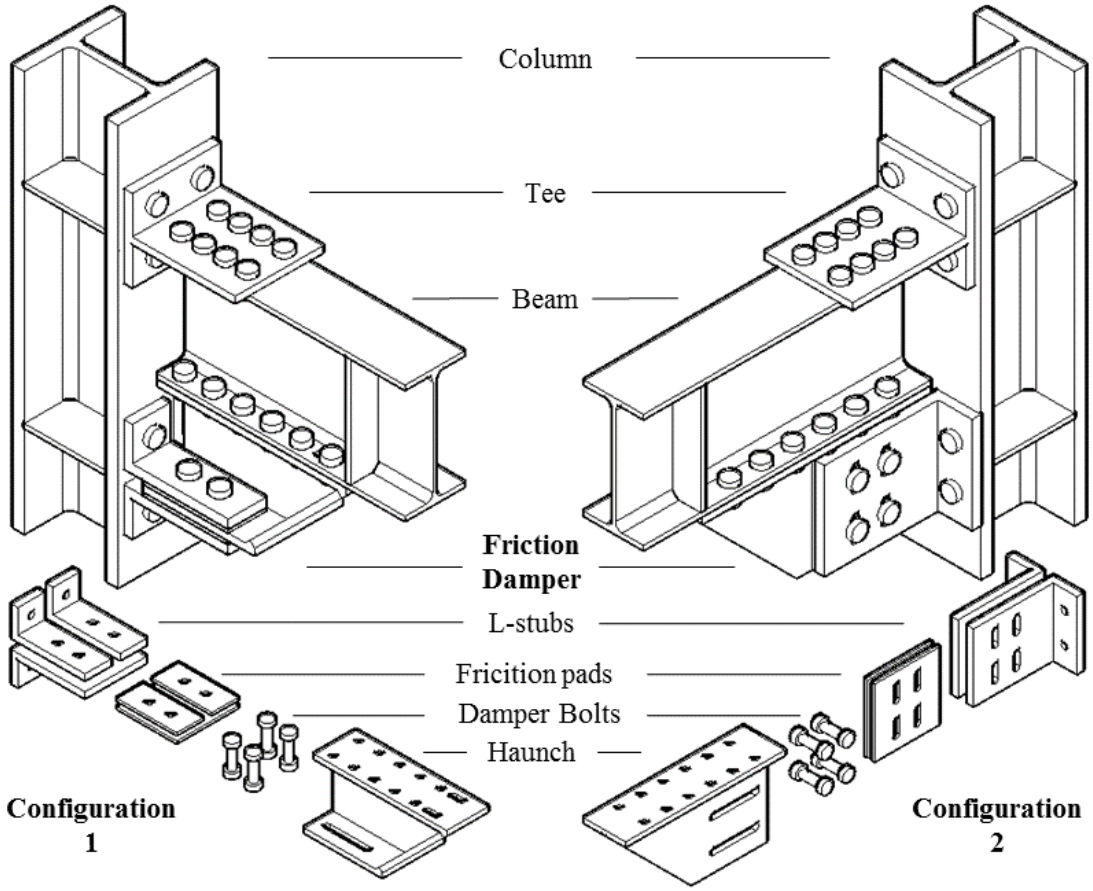


Figure 1 FREEDAM joint configurations

The interactions between the surfaces in contact (e.g. bolt-to-plates, plate-to-plate) are modelled considering both "Normal" and "Tangential" behaviour. The former is implemented considering "Hard Contact", while the latter is modelled differently for the steel–to-steel interfaces and for the friction pad- to–steel interfaces. The main difference between the two types of contacts is the definition of the friction coefficient. For the steel-to-steel surfaces a constant value equal to 0.3 is considered, while the dynamic friction coefficients obtained from lap-shear tests with the friction material considered are used for the friction damper (see Table 1).

The clamping of the bolts is modelled by means of the "Bolt load" option available in the FE software.

The boundary conditions are modelled to be representative of those adopted for the experimental set-up (see Figure 2). Both column ends have translational and rotational degrees of freedom restrained with the exception of the in-plane rotation, and the beam is restrained to prevent the lateral-torsional buckling. The loads are applied in the section corresponding to the actual position of the actuator 1. Both monotonic and cyclic displacement histories are alternatively applied. The AISC 341-16 loading protocol [44] is used for cyclic tests and numerical analyses.

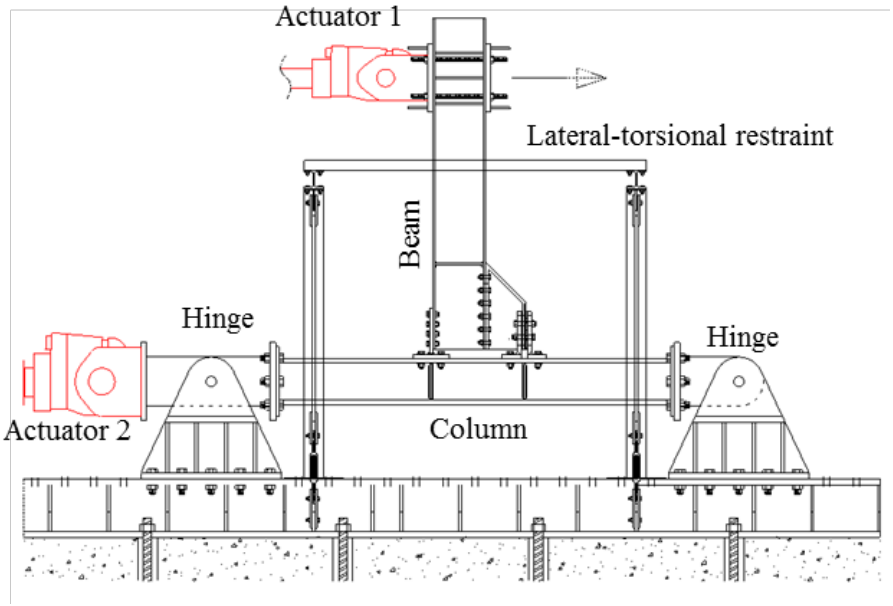


Figure 2 Experimental set-up

Dynamic implicit quasi-static analyses are performed considering two subsequent steps: i) the bolt clamping is first applied; 2) the displacement history is applied at the beam tip.

## 2.2 FE blind predictions vs experimental response

In order to evaluate the fitness of the modelling assumptions, the results of preliminary analyses simulating the experimental conditions (i.e. the design friction coefficient is the dynamic 5% fractile equal to 0.53 and damper-side bolt clamping considered as in Table 2) are compared with the results of experimental tests performed at the University of Salerno within FREEDAM project [41].

Figure 3 and Figure 4 depict the comparison between the FE analyses and the cyclic tests in terms of response curves (i.e. bending moment at the column axis and chord rotation) and failure mode, respectively. As it can be recognized, the simulated response accurately reproduces the experimental behaviour. However, the models do not reproduce the first cycles due to the simplified friction interaction law, where static friction coefficient is not accounted for. The larger difference observed for the joint configuration 2 is caused by the variations between the design and actual values of both the friction coefficient and the clamping forces of the bolts.

FE analyses confirm the experimental observations, namely no significant damage occurs even though the numerical models show some localization of damage in the base of the webs of both Tee and L-stubs. However, the equivalent plastic strain (PEEQ) are very small and fully acceptable for large rotational demands.

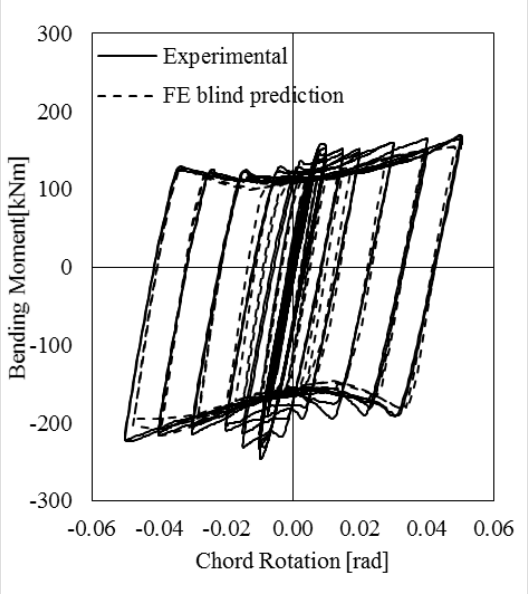


a) Configuration 1

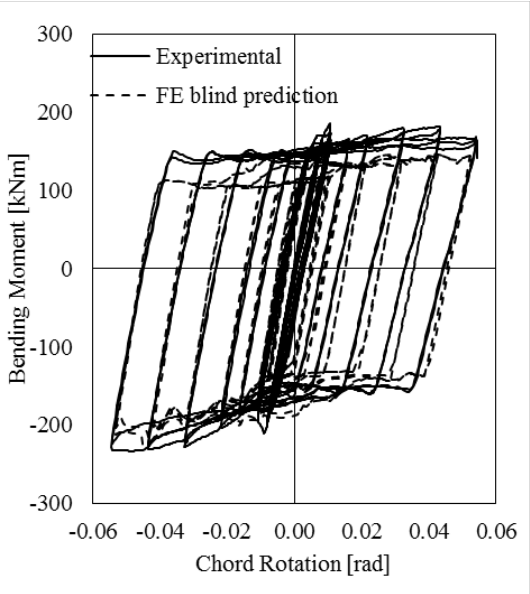


b) ) Configuration 2

Figure 3 Comparison of numerical blind predictions and experimental test results

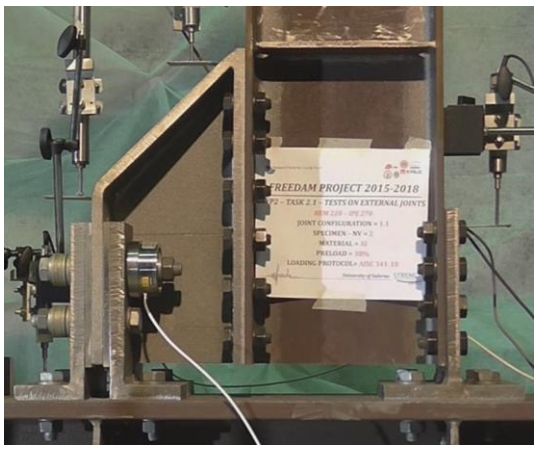

a) Experimental joint FD 1-1

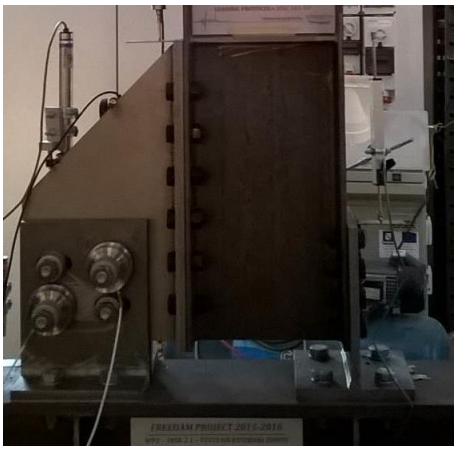

b) Experimental joint FD 2-1

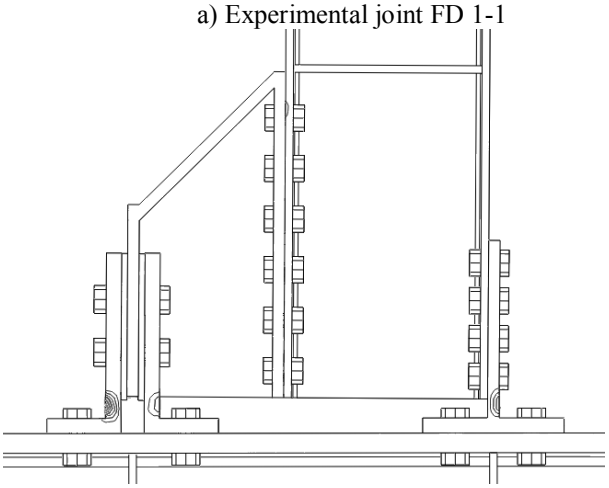

c) PEEQ distribution for model FD 1-1

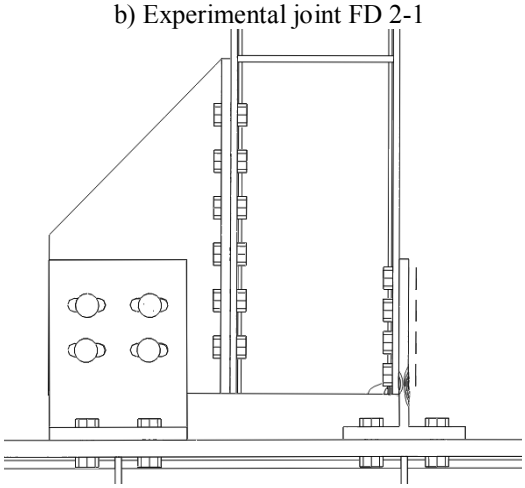

d) PEEQ distribution for model FD 2-1

Figure 4 Experimental vs. numerical models after cyclic test up to 5%

# 3 PARAMETRIC ANALYSIS

## 3.1 Investigated parameters

The mechanical parameters investigated for the two types of joint configurations are the followings:

- Friction Coefficient. Three values of the dynamic friction coefficient $\mu$ are considered: the 5% percentile ($\mu_{5\%}$ - which is also the value used for the design of the friction damper), the average value ($\mu_{avg}$) and the 95% percentile ($\mu_{95\%}$).

| | $\mu_{5\%}$ | $\mu_{avg}$ | $\mu_{95\%}$ |
|---|---|---|---|
| Friction Material M-1 | 0.53 | 0.59 | 0.64 |

Table 1 Friction coefficient

- Clamping force. Three values of bolt pre-tensioning $N_b$ are assumed – the design value (denoted $N_b$ in Table 2), a value 50% smaller (0.5 $N_b$) and a value 50% larger (1.5 $N_b$). In Table 2 $n_b$ represents the percentage of clamping force with respect to $F_{p,C}$, the design clamping force recommended by EC 3 1-8 [45]. It should be noted that in all cases 1.5 $N_b$ is smaller than $F_{p,C}$ (which is equal to 172kN for M20 gr.10.9 bolts).

| | $n_b$ [%] | $N_b$ [kN] |
|---|---|---|
| FD 1-1 | 34% | 58 |
| FD 1-2 | 57% | 99 |
| FD 2-1 | 37% | 63 |
| FD 2-2 | 61% | 105 |

Table 2 Design values of clamping force $N_b$

The models used for the parametric investigation are identified on the basis of the scheme reported in Figure 5. The beam-to-column assemblies of both configurations are made-up of the following beam-column pairs: IPE 270 – HE 220M (1) and IPE 450 – HE 500B (2)


Figure 5 Model name definition

The results of the parametric study are presented in terms of bending moment – chord rotation curves, both for hogging (negative values) and sagging (positive values) loading conditions.

## 3.2 Clamping force

The bending resistance of the joints depends on the clamping forces in the bolts of the friction damper. Figure 6 shows the comparison of the response curves for all four models (i.e. the two joint configurations and two assemblies) and Table 3 and Table 4 report the mechanical properties of the joints. The bending moments reported, $M^{(+)}$ and $M^{(-)}$, represent the bending moment at the occurrence of the sliding under sagging and hogging. Equations (1), (2) and (3) define the way the values in the tables were obtained.

$$\Gamma^{(+)} = 1 + \frac{M^{(+)}_{0.5N_b} - M^{(+)}_{N_b}}{M^{(+)}_{N_b}} \tag{1}$$

$$\Gamma^{(-)} = 1 + \frac{M^{(-)}_{0.5N_b} - M^{(-)}_{N_b}}{M^{(-)}_{N_b}} \tag{2}$$

$$\Delta M^{(+/-)} / M^{(-)} = \frac{M^{(-)} - M^{(+)}}{M^{(-)}} \tag{3}$$

Where:

$\Gamma^{(+)}$ and $\Gamma^{(-)}$ are the hogging and sagging bending moment capacity, respectively, considering alternatively the change in the clamping force from the design value $N_b$ to 0.5 $N_b$ and 1.5 $N_b$.

$M^{(+)}$ and $M^{(-)}$ are the sagging and hogging bending moments. The subscripts depict the analysis from which the bending moment is taken, e.g. with clamping force equal to either $N_b$ or 0.5 $N_b$.

$\Delta M^{(+/-)}/M^{(-)}$ provides the variation of bending moment (either hogging and sagging) as respect to those exhibited by the joints with bolts clamped at $N_b$.

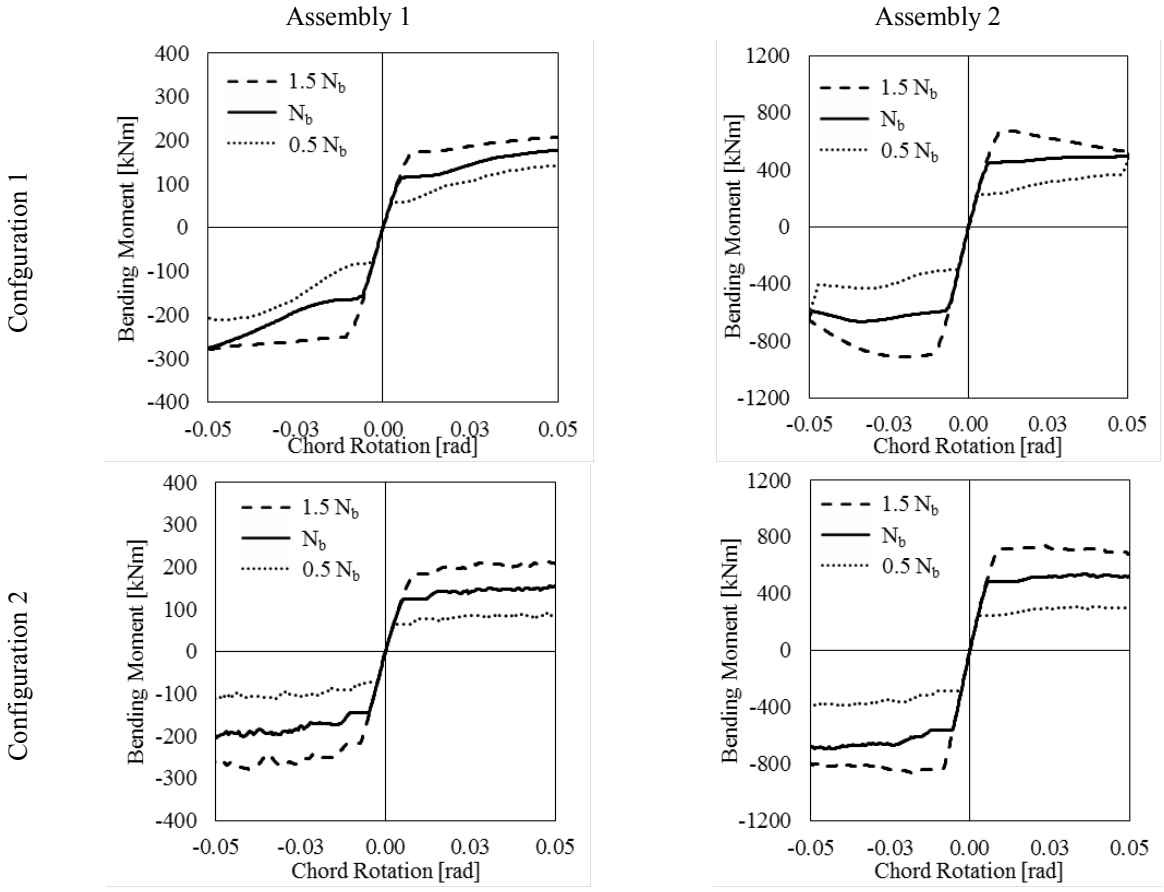


Figure 6 Influence of the clamping force on the bending moment capacity

For all examined cases, the reduction/magnification of the bending moment is proportional with the bolt pre-tension under both sagging and hogging. This outcome confirms that the bending moment capacity depends linearly on the tightening force in the bolts.

As reported in Table 3 and Table 4, this difference is strictly related to the joint configuration and it is constant with the beam depths, clamping force, or friction coefficient. The difference is about 25% for Configuration 1 and 15% for configuration 2.

Further observation that can be made based on Figure 6 is that the post-yield response of joint configuration 1 differs with the size of the beam-to-column assembly. In particular, the joint with shallow beam exhibits hardening (i.e. positive post-yield stiffness), while the joint with deep beam shows softening (i.e. negative post-yield stiffness), the latter is more evident for the lower values of clamping force. These phenomena are more pronounced under hogging bending moment. The second configuration exhibits a more linear behaviour in both examined assemblies.

The stiffness of the joint is not affected by the variation of clamping force, since it is determined by the stiffness of the other components of the joint (the connection at column face, the column web panel, etc.).

| FD 1-2 | $M^{(+)}$ [kNm] | $M^{(-)}$ [kNm] | $\Gamma^{(+)}$ [-] | $\Gamma^{(-)}$ [-] | $\Delta M^{(+/-)}/M^{(-)}$ [-] |
|---|---|---|---|---|---|
| $N_b$ | 453 | 602 | | | 25% |
| $0.5N_b$ | 230 | 298 | 51% | 50% | 23% |
| $1.5N_b$ | 690 | 902 | 152% | 150% | 24% |

Table 3 Bending moments for model FD 1-2 considering the variation of clamping force

| FD 2-2 | $M^{(+)}$ [kNm] | $M^{(-)}$ [kNm] | $\Gamma^{(+)}$ [-] | $\Gamma^{(-)}$ [-] | $\Delta M^{(+/-)}/M^{(-)}$ [-] |
|---|---|---|---|---|---|
| $N_b$ | 484 | 564 | | | 14% |
| $0.5N_b$ | 250 | 290 | 52% | 51% | 14% |
| $1.5N_b$ | 714 | 838 | 148% | 149% | 15% |

Table 4 Bending moments for model FD 2-2 considering the variation of clamping force

### 3.3 Friction Coefficient

The variability of the friction coefficient $\mu$ influences the bending moment capacity of the joints. The experimental campaign carried out on lap shear splices at the University of Salerno allowed characterizing the probabilistic distribution of this parameter. The FE analyses are carried out on the basis of the obtained percentiles of $\mu$ that are reported in Table 1. Figure 7 depicts the numerical curves in terms of bending moment-chord rotation. It is possible to observe that the higher friction coefficient fractile values the larger is the joint capacity. This observation confirms the need to account for the variability of the friction properties of the friction pads to design the non-dissipative structural members.

Similar hardening/softening behaviour can be observed for both joint configuration and, additionally, the response curves seem scaled proportionality with the friction coefficient.

Table 5 and Table 6 depict the variation of the bending capacity of the FD 1-2 and FD 2-2 models analysed with larger values of friction coefficient ($\mu_{avg}$ and $\mu_{95\%}$) with respect to the design value ($\mu_{5\%}$) under hogging ($M^{(-)}$) and sagging ($M^{(+)}$) loading conditions. The variation in case of FD 1-2 differs with respect to the variation of the friction coefficient. In particular, a larger increase of bending moment can be observed for the same increase of friction coefficient. On the other side, the analyses of model FD 2-2 in Table 6 show a closer dependency of the bending capacity with the friction property randomness.

| FD 1-2 | $\Delta\mu$ [-] | $M^{(+)}$ [kNm] | $M^{(-)}$ [kNm] | $\Gamma^{(+)}$ [-] | $\Gamma^{(-)}$ [-] | $\Delta M^{(+/-)}/M^{(-)}$ [-] |
|---|---|---|---|---|---|---|
| $\mu_{5\%}$ | | 446 | 593 | | | 25% |
| $\mu_{avg}$ | 110% | 521 | 670 | 117% | 113% | 22% |
| $\mu_{95\%}$ | 117% | 535 | 733 | 120% | 124% | 27% |

Table 5 Bending moments for model FD 1-2 considering the friction coefficient variation

| FD 2-2 | $\Delta\mu$ [-] | $M^{(+)}$ [kNm] | $M^{(-)}$ [kNm] | $\Gamma^{(+)}$ [-] | $\Gamma^{(-)}$ [-] | $\Delta M^{(+/-)}/M^{(-)}$ [-] |
|---|---|---|---|---|---|---|
| $\mu_{5\%}$ | | 484 | 564 | | | 14% |
| $\mu_{avg}$ | 110% | 529 | 627 | 109% | 111% | 16% |
| $\mu_{95\%}$ | 117% | 568 | 679 | 117% | 120% | 16% |

Table 6 Bending moments for model FD 2-2 considering the friction coefficient variation

The parameter $\Delta M^{(+/-)}/M^{(-)}$, evaluated also for this set of analyses confirms the previous observation regarding the relation between the damper's configuration and the different response under sagging and hogging conditions (values ranging around 25% for configuration 1 and 15% for configuration 2).

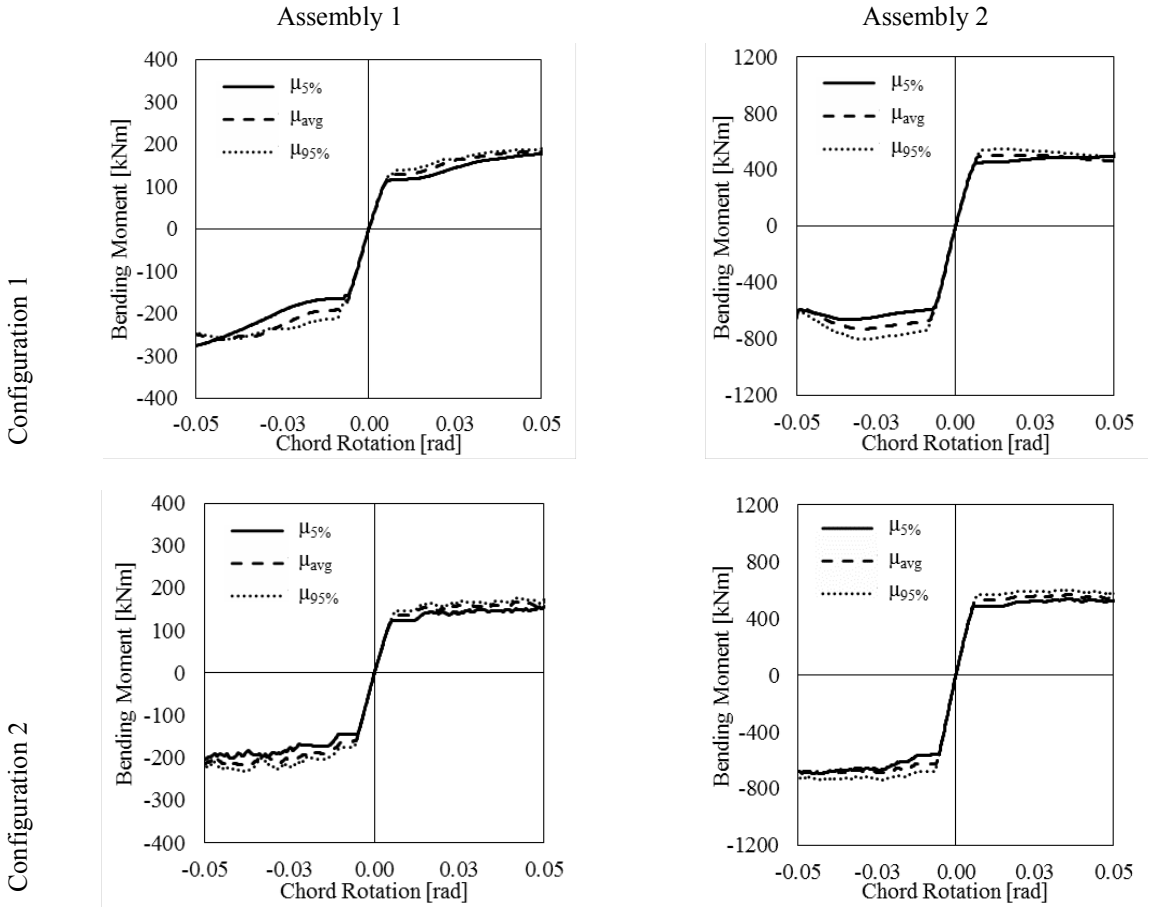


Figure 7 The influence o the friction coefficient on the bending moment resistance

## 4 CONCLUSIONS

This paper summarizes the results of parametric finite element simulations on two types of innovative friction based dissipative beam-to-column joints. Based on the discussion of the numerical outcomes, the following remarks can be drawn:

- The FE models accurately predict the response of experimental tests.
- The variation of the bending capacity of both joint configurations is directly proportional with the bolt pretension force. Therefore, the bolt tightening process needs to be very well controlled because either larger or smaller tightening forces can impair the proper dissipative mechanisms. Indeed, the upper bound values lead to the development of larger forces in the damper, situation that hinders the hierarchy in the joint, while lower clamping forces can lead to sliding in the damper under serviceability conditions.
- The randomness of the friction properties has to be as much as possible mitigated and accounted for in the design phase, because this variability can inflict in the joint response and, consequently, the global behaviour of the structure.
- The joint configuration dictates the level of the response symmetry under sagging and hogging bending.

## REFERENCES

[1] F.M. Mazzolani, V. Piluso. Plastic design of seismic resistant steel frames. *Earthquake Engineering and Structural Dynamics*, **26 (2)**, 167-191, 2017.

[2] R. Montuori, E. Nastri, V. Piluso. Theory of Plastic Mechanism Control for MRF-EBF dual systems: Closed form solution. *Engineering Structures*, **118**, 287-306, 2016.

[3] R. Montuori, E. Nastri, V. Piluso. Theory of plastic mechanism control for eccentrically braced frames with inverted y-scheme. *Journal of Constructional Steel Research*, **92**, 122-135, 2014.

[4] D. Cassiano, M. D'Aniello, C. Rebelo, R. Landolfo, L. da Silva. Influence of seismic design rules on the robustness of steel moment resisting frames. *Steel and Composite Structures, An International Journal*, **21(3)**, 479-500, 2016.

[5] A. Tenchini, M. D'Aniello, C. Rebelo, R. Landolfo, L. da Silva, L. Lima. High strength steel in chevron concentrically braced frames designed according to Eurocode 8. *Engineering Structures,* **124**, 167–185, 2016.

[6] M. D'Aniello, R. Tartaglia, S. Costanzo, R. Landolfo. Seismic design of extended stiffened end-plate joints in the framework of Eurocodes. *Journal of Constructional Steel Research*, **128**, 512-527, 2017.

[7] A. Tenchini, M. D'Aniello, C. Rebelo, R. Landolfo, L. da Silva, L. Lima. Seismic performance of dual-steel moment resisting frames. *Journal of Constructional Steel Research*, **101**, 437-454, 2014.

[8] A. Tenchini, M. D'Aniello, C. Rebelo, R. Landolfo, L. da Silva, L. Lima. High strength steel in chevron concentrically braced frames designed according to Eurocode 8. *Engineering Structures* **124**, 167–185, 2016.

[9] R. Tremblay, P. Timler, M. Bruneau, and A. Filiatrault, Performance of steel structures during the 1994 Northridge earthquake, *Journal of Civil Engineering*, **22**, 338-60, 1995.

[10] N. Youssef, D. Bonowitz, and J. Gross, *A Survey of Steel Moment-Resisting Frame Buildings Affected by the 1994 Northridge Earthquake, Research report no. NISTIR*

*5625*. National Institute of Science and Technology (NIST), Gaithersburg (MD, USA), 1995.

[11] FEMA 350, "Recommended Seismic Design Provisions for New Moment Frame Buildings Report," Federal Emergency Management Agency, Washington DC, 2000

[12] M. Nakashima, K. Inoue, and M. Tada, Classification of damage to steel buildings observed in the 1995 Hyogoken-Nanbu earthquake, *Engineering Structures*, **20**, 271-81, 1998.

[13] E. Watanabe, K. Sugiura, K. Nagata, and Y. Kitane, Performances and damages to steel structures during 1995 Hyogoken-Nanbu earthquake, *Engineering Structures*, **20**, 282-90, 1998.

[14] E. M. Güneyisi, Seismic reliability of steel moment resisting framed buildings retrofitted with buckling restrained braces, *Earthquake Engineering and Structural Dynamics*, **41**, 853-74, 2012.

[15] M. Bosco, and E.M. Marino, Design method and behavior factor for steel frames with buckling restrained braces, *Earthquake Engineering & Structural Dynamics*, **42**, 1243-63, 2013.

[16] G. Della Corte, M. D'Aniello, and R. Landolfo, Field testing of all-steel buckling restrained braces applied to a damaged reinforced concrete building, *Journal of Structural Engineering,* **141(1)**, D4014004, 2015.

[17] M. D'Aniello, G. Della Corte, F.M. Mazzolani. Experimental tests of a real building seismically retrofitted by special buckling-restrained braces. *2008 Seismic Engineering Conference Commemorating the 1908 Messina and Reggio Calabria Earthquake*, Reggio Calabria, Italy, July 8-11, 2008.

[18] G. De Matteis, A. Formisano, F.M. Mazzolani and S. Panico, Design of low-yield metal shear panels for energy dissipation. *The Final Conference of COST Action C12*, Innsbruck, Austria, January 20-22, 2005.

[19] A. Formisano, A.G. De Matteis and F.M. Mazzolani, Numerical and experimental behaviour of a full-scale RC structure upgraded with steel and aluminum shear panels. *Computers and Structures*, **88 (23-24)**, 1348-1360, 2010.

[20] B. Dong, R. Sause, J. M. Ricles, Seismic Response of a steel MRF Building with Nonlinear viscous dampers under DBE and MCE. *J Struct Eng*, **142(0)** 1-1, 2010.

[21] A. S. Tzimas, G. S. Kamaris, T.L. Karavasilis, C. Galasso, Collapse risk and residual drift performance of steel buildings using post-tensioned MRFs and viscous dampers in near-fault regions. *Bull Earthquake Eng.*, **14**, 1643–1662, 2016.

[22] T. L. Karavasilis, Assessment of capacity design of columns in steel moment resisting frames with viscous dampers. *Soil Dynamics and Earthquake Engineering* **88**, 215–222, 2016

[23] A. Ioan, A. Stratan, D. Dubina, M. Poljansek, F. J. Molina, F. Taucer, P. Pegon, G. Sabau, Experimental validation of re-centering capability of eccentrically braced frames with removable links. *Engineering Structures*, **113**, 335-346, 2016.

[24] F.M. Mazzolani, G. Della Corte and M. D'Aniello, Experimental analysis of steel dissipative bracing systems for seismic upgrading. *Journal of Civil Engineering and Management*, **15**, 7-19, 2009.

[25] M. D'Aniello, G. Della Corte, F.M. Mazzolani, Seismic Upgrading of RC Buildings by Eccentric Braces: Experimental Results vs. Numerical Modelling. STESSA Conference 2006, Tokyo, Japan, August 14-17, 2006.

[26] E. Barecchia, M. D'Aniello, G. Della Corte, F.M. Mazzolani. Eccentric bracing in seismic retrofitting: from full scale tests to numerical FEM analysis. *International Conference On Metal Structures 2006 "Steel - A New And Traditional Material For Building"* Poiana Braşov, Romania, September 20-22, 2006.

[27] M. Latour, G. Rizzano. Full strength design of column base connections accounting for random material variability. *Engineering Structures*, **48**, 458-471, 2013.

[28] M. Latour, G. Rizzano. A theoretical model for predicting the rotational capacity of steel base joints. *Journal of Constructional Steel Research*, **91**, 89-99, 2013.

[29] M. Latour, G. Rizzano, A. Santiago, L.S. da Silva. Experimental analysis and mechanical modeling of T-stubs with four bolts per row. *Journal of Constructional Steel Research*, **101**, 158-174, 2014.

[30] M. Latour, G. Rizzano. Cyclic behavior and modeling of a dissipative connector for cross-laminated timber panel buildings. *Journal of Earthquake Engineering*, **19 (1)**, 137-171, 2015.

[31] M. Latour, V. Piluso, G. Rizzano. Rotational behaviour of column base plate connections: Experimental analysis and modelling. *Engineering Structures*, **68**, 14-23, 2014.

[32] L. Feo, M. Latour, R. Penna, G. Rizzano. Pilot study on the experimental behavior of GFRP-steel slip-critical connections. *Composites Part B: Engineering*, 2017 (in Press)

[33] E. M. Guneyisi, M. D'Aniello, R. Landolfo, Seismic upgrading of steel Moment-Resisting Frames by means of friction devices. *The Open Construction and Building Technology Journal*, **8** (Suppl 1: M9), 289-299, 2014.

[34] V. Piluso, R. Montuori, M. Troisi, Innovative structural details in MR-frames for free from damage structures, *Mechanics Research Communications* **58,** 146-156, 2014.

[35] M. Taghi Nikoukalam, S. R. Mirghaderi and K. M. Dolatshahi, Analytical Study of Moment-Resisting Frames Retrofitted with Shear Slotted Bolted Connection, *J. Struct. Eng*. 04015019

[36] H-H. Khoo, C. Clifton, J. Butterworth, G. MacRae, G. Fergurson, Influence of steel shim hardness on the sliding hinge joint performance. *Journal of Constructional Steel Research* **72**, 119-129, 2012.

[37] H-H. Khoo, C. Clifton, J. Butterworth, G. MacRae, Experimental Study of Full-Scale Self-Centering Sliding Hinge Joint Connections with Friction Ring Springs. *Journal of Earthquake Engineering* **17(7)**, 972-997, 2013.

[38] M. Latour, V. Piluso and G. Rizzano, Experimental Analysis on Friction Materials for Supplemental Damping Devices. *Construction and Building Materials*, **65,** 159-176, 2014.

[39] M. Latour, V. Piluso and G. Rizzano, Free from damage beam-to-column joints: Testing and design of DST connections with friction pads, *Engineering Structures* **85**, 219–233, 2015.

[40] G. Ferrante Cavallaro, A. Francavilla, M. Latour, V. Piluso, G. Rizzano. Experimental behaviour of innovative thermal spray coating materials for FREEDAM joints. *Composites Part B: Engineering*, 2017 (in Press).

[41] Research Fund for Coal and Steel (RFCS) research programme under grant agreement n° RFSR-CT-2015-00022 FREE from DAMage Steel Connections (FREEDAM).

[42] Dassault (2014), Abaqus 6.14 - Abaqus Analysis User's Manual, Dassault Systèmes Simulia Corp.

[43] M. D'Aniello, D. Cassiano and R. Landolfo, Monotonic and cyclic inelastic tensile response of European preloadable gr10.9 bolt assemblies, *Journal of Constructional Steel Research*, **124**, 77–90, 2016.

[44] ANSI/AISC 341-16 (2016). "Seismic Provisions for Structural Steel Buildings". American Institute of Steel Construction.

[45] EN 1993:1–8, Design of Steel Structures - Part 1–8: Design of Joints. CEN, 2005.